



Invasion percolation in short-range and long-range disorder background

M. N. Najafi,^{1,*} S. Tizdast,¹ J. Cheraghalizadeh¹ ,¹ and H. Dashti N.²

¹*Department of Physics, University of Mohaghegh Ardabili, P.O. Box 179, Ardabil, Iran*

²*School of Physics, Korea Institute for Advanced Study, Seoul 02455, Korea*

 (Received 10 May 2021; revised 18 October 2021; accepted 23 November 2021; published 14 December 2021)

In the original invasion percolation model, a random number quantifies the role of necks, or generally the quality of pores, ignoring the structure of pores and impermeable regions (to which the invader cannot enter). In this paper, we investigate invasion percolation (IP), taking into account the impermeable regions, the configuration of which is modeled by ordinary and Ising-correlated site percolation (with short-range interactions, SRI), on top of which the IP dynamics is defined. We model the long-ranged correlations of pores by a random Coulomb potential (RCP). By examining various dynamical observables, we suggest that the critical exponents of Ising-correlated cases change considerably only in the vicinity of the critical point (critical temperature), while for the ordinary percolation case the exponents are robust against the occupancy parameter p . The properties of the model for the long-range interactions [LRI (RCP)] are completely different from the normal IP. In particular, the fractal dimension of the external frontier of the largest hole is nearly $\frac{4}{3}$ for SRI far from the critical points, which is compatible with normal IP, while it converges to 1.099 ± 0.04 for RCP. For the latter case, the time dependence of our observables is divided into three parts: the power law (short time), the logarithmic (moderate time), and the linear (long time) regimes. The second crossover time is shown to go to infinity in the thermodynamic limit, whereas the first crossover time is nearly unchanged, signaling the dominance of the logarithmic regime. The average gyration radius of the growing clusters, the length of their external perimeter, and the corresponding roughness are shown to be nearly constant for the long-time regime in the thermodynamic limit.

DOI: [10.1103/PhysRevE.104.064119](https://doi.org/10.1103/PhysRevE.104.064119)

I. INTRODUCTION

Invasion percolation (IP) [1,2] was first introduced in 1983 by Wilkinson and Willemsen (WW) to describe the slow displacement of one fluid by another *invader* in porous media [2]. IP is the invasion phenomenon during which one phase invades the other one in a porous medium. Invasion percolation is divided into two general categories: trapping invasion percolation and nontrapping invasion percolation, in which the defender fluid is incompressible and compressible, respectively [3]. In a lattice setup, this model is simple to define: One fills the system with the defender fluid and then the invader fluid (displacement) is injected into the environment. In the original version of this model, an uncorrelated uniform random number r quantifies the quality of the pores and necks without taking into account the configuration of *impermeable regions*. Therefore, the stochasticity of fluid movement (due to stochastic properties of the voids in the porous media) is realized by $\{r_i\}_{i=1}^N$, where i shows the sites on the lattice and N is the system size. The main difference between IP and ordinary percolation is that it automatically organizes itself in a critical point, for which one uses the term self-organized criticality [4,5]. Many aspects and properties of IP are known in the community. The most important example is the well-known fact that the fractal structure of

IP clusters (the cluster that is formed by invaded sites) is just similar to the one for the standard (site) percolation; e.g., the fractal dimension of the external frontier of the largest hole is $D_f = \frac{4}{3}$ [6–8]. The other examples are three-dimensional IP [9], IP in correlated porous media [10,11], fractal growth dependence on the coordination number [12], and many applications in reservoir engineering [13]. Recently it was demonstrated that, apart from the dynamical power-law behaviors, IP shows a dynamical crossover during which the autocorrelation change sign [14]. For a good review of the theoretical and experimental development of IP, see Ref. [15].

Despite the intense focus on the various variants of IP and exploring its features and properties [12,14,16,17], the effect of the pattern of the background has not been understood well yet. By “the pattern of background,” we mean the pattern of impermeable sites. Its impact on the statistical properties of the growing invasion cluster is a question that has not been addressed yet in the literature. The important fact that makes the IP model far from real situations (and the useful reservoir models like the Darcy model) is that it ignores the structure of media involving impermeable pores, especially the effect of the correlations, the effect of which is not known *a priori* [18–20]. It is the aim of this paper to consider a wider range of models to capture the correlations in the support for two categories: short-range interaction (SRI) models and long-range interaction (LRI) models. One may call our model the hierarchical percolation: the invasion percolation on top

*morteza.nattagh@gmail.com

of the percolation lattice. Three kinds of configurations are considered: (1) uncorrelated percolation, (2) Ising-correlated percolation, and (3) imperfections with long-range interactions (RCP). The interactions in the first two models are of short-range nature, while the third model is pretty long range. When the correlated lattices are constructed, we run the IP dynamics on top of them, avoiding the fluid entering the impermeable regions (sites in our model). The coupling of two independent statistical models (one dynamical model on top of another host model) has been previously done for sand piles on uncorrelated percolation lattice [21,22] and Ising-correlated percolation lattice [23,24], Gaussian free field on percolation lattices [25,26], Ising model on percolation and Ising-correlated percolation lattices [24,27], and self-avoiding walk on correlated lattices [28]. The main question from this point of view is the universality class that the resulting models belong to.

The paper has been organized as follows: In the next section, the simulation performed is described. In the third section, we will describe and present numerical details and simulation results. We will close the paper with a conclusion. The paper includes an Appendix.

II. GENERAL SETUP OF THE PROBLEM

In the original version of the IP model, one distributes a uniform random number r throughout the lattice and lets the interface of the invader grow according to the configuration of r on the boundary of the invasion cluster: The invader continues to move from a site with a minimum r value. As WW discusses, when one requires that the invader goes ahead from all sites on the boundary of the invasion cluster, with $r < p$ (p being a fixed number), then one retrieves the ordinary percolation model with the occupancy number p . To strengthen the relation to the ordinary percolation, the authors study $a(r)$, which is the number of sites included in the invasion cluster in the interval $[r, r + dr]$, divided by dr , and show that it undergoes a transition at p_c (the critical threshold of ordinary percolation). In fact, in the original version of the invasion percolation, the properties of porous media are coded in the configuration of r field.

A. The IP model on imperfect systems

In experiments, correlations are due to the formation process (slow dynamics) during which the various parts of the host system interact. Consider, for example, the sedimentation process where the constituents interact with each other via the interface relaxation process [29]. As a well-known fact, the porous media is formed by the sedimentation process during which some parts become permeable to the fluid and some others are impermeable, which we call the permeability field (PF). This process can be accompanied by long-range or short-range interactions, resulting in a quenched disorder system after millions of years, for which there are correlations. It is not physically reasonable to use one kind of model (e.g., the uncorrelated percolation) for all the porous medium. To realize the physics of this system, it is necessary and important to use models with various kinds of interactions. The state of a porous media is then partially described by PF, and knowing

the pattern of it helps in any prediction of the model that is employed to simulate the fluid propagation. The effect of the correlated configuration of PF has not been convincingly understood yet in the literature and very limited attention has been paid to this issue, like IP in fractional Gaussian noise [10,11,30,31].

To describe our model, suppose that in addition to the necks or the quality of the pores, there are some impermeable regions to which the invader cannot enter. These forbidden areas are neglected in the original IP model, the effect of which is not known *a priori*. Let us call these regions imperfections. The configuration of the imperfections matters, as we show in the paper. Three kinds of configurations are considered: (1) uncorrelated percolation, (2) Ising-correlated percolation, and (3) imperfections with long-range interactions (RCP). The first two cases are short-range interactions, while the third contains long-range interactions. The host lattice is the infiltration lattice for each statistical model defined on it. These studies have many natural and objective examples in which the dynamics of the influence lattice are defined [18–20]. Our model is defined on an $L \times L$ square lattice with permeable and impermeable sites. The pattern of impermeable sites (imperfections) is determined by three models in this paper: percolation, Ising, and RCP models. For the percolation and Ising models (SRI supports), the sites can have two possible states, represented by $s_i = +1$ or -1 , showing that the site i is permeable or impermeable, respectively, whereas for the RCP $s_i = +1$ for all sites. The fluid can only pass through permeable sites, i.e., the clusters comprising sites with $s_i = +1$. For the SRI supports (Ising- and percolation-correlated lattices), the configuration of $\{s_i\}_{i=1}^{L^2}$ is fixed using the Ising and site percolation models respectively, whereas for the LRI the configurations of r_i s are given by RCP. We describe these models in the following subsection. IP is run over the largest percolating connected cluster (PCC, comprised of $s = +1$ sites) with total N sites, which is a cluster that connects two opposite boundaries of the lattice (for the RCP case, it is actually the original lattice). Once a PCC is extracted, the IP growth model is defined on top of it, defined as follows: N uncorrelated random numbers r in the range $[0,1]$ are distributed over the PCC so that the state of the porous media is identified by $\{r_i\}_{i=1}^N$. The dynamics start from a middle point of the lattice i_0 (if it does not belong to the percolating cluster, we move in a random direction and consider the first site belonging to the PCC as the starting point) where the fluid is injected. At the next step, the invader moves to a neighbor of the injected point (say the site j) with the smallest r , i.e., $r_j = \min\{r_i\}_{i \in \partial S(1)}$, where $S(m)$ is the set of the infected (filled by the invader) sites up to the step m , and ∂S is the set of neighbors of the infected sites S . If two or more neighbors are equal in the parameter r , one of these minimums is randomly chosen. In the step $m + 1$, the fluid enters the site $j \in \partial S(m)$, which is identified by the condition $r_j = \min\{r_i\}_{i \in \partial S(m)}$ (if there are more, it is selected randomly between the set of neighboring sites with minimum r). The “time” is defined as the integer part of $\frac{m}{10}$. The process goes ahead until two opposite boundaries are touched by $S(m_{\max})$. In the ordinary IP, a phase transition occurs at this point to a phase where the invader fills the space, where IP shows

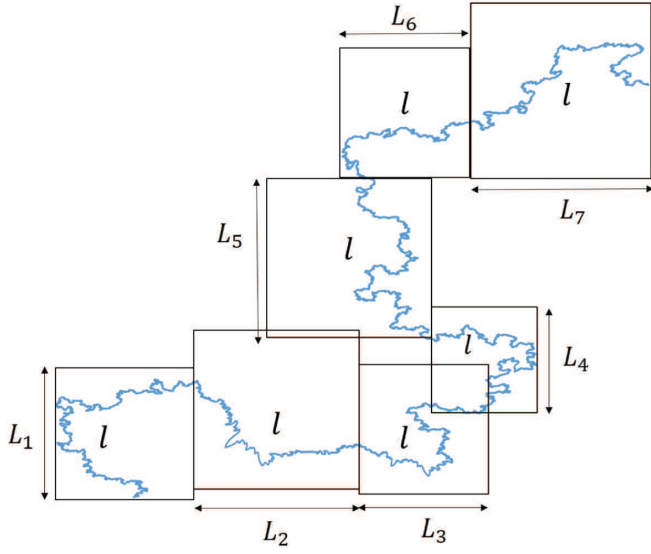


FIG. 1. The procedure of calculating the fractal dimensional (box-counting).

power-law behavior [14]. This IP has the same properties as the ordinary site percolation at the critical point. IP shows also power behavior with respect to time for various observables, and there are some scaling relations between the quantities.

The quantities that we analyze here are as follows:

(1) The loop length (l) is defined as the length of the loop surrounding the cluster, so that $l(t) \equiv \sum_{j=1}^N \delta_{j, \partial S(t)}$, where $\delta_{j, \partial S} = 1$ when $j \in S$, and zero otherwise; i.e., it is the number of sites on the boundary of $S(t)$.

(2) The loop and mass gyration radii [$r_l(t)$ and $r_m(t)$ respectively] are defined by

$$r_l(t)^2 = \frac{1}{l(t)} \sum_{i \in \partial S(t)} [(x_i - \bar{x}_l)^2 + (y_i - \bar{y}_l)^2],$$

$$r_m(t)^2 = \frac{1}{S(t)} \sum_{i \in S(t)} [(x_i - \bar{x}_m)^2 + (y_i - \bar{y}_m)^2], \quad (1)$$

where x_i and y_i are the Cartesian coordinates of the site i , (\bar{x}_l, \bar{y}_l) is the loop center, and (\bar{x}_m, \bar{y}_m) is the mass center, defined as

$$(\bar{x}_l, \bar{y}_l) \equiv \frac{1}{l(t)} \sum_{i \in \partial S(t)} (x_i, y_i), \quad (\bar{x}_m, \bar{y}_m) \equiv \frac{1}{S(t)} \sum_{i \in S(t)} (x_i, y_i). \quad (2)$$

(3) The roughness (w) is defined by

$$w(t)^2 = \frac{1}{l(t)} \sum_{i \in \partial S(t)} (r_i - \bar{r})^2, \quad (3)$$

where $r_i \equiv (x_i^2 + y_i^2)^{\frac{1}{2}}$ and $\bar{r} \equiv \frac{1}{l(t)} \sum_{i \in \partial S(t)} (x_i^2 + y_i^2)^{\frac{1}{2}}$.

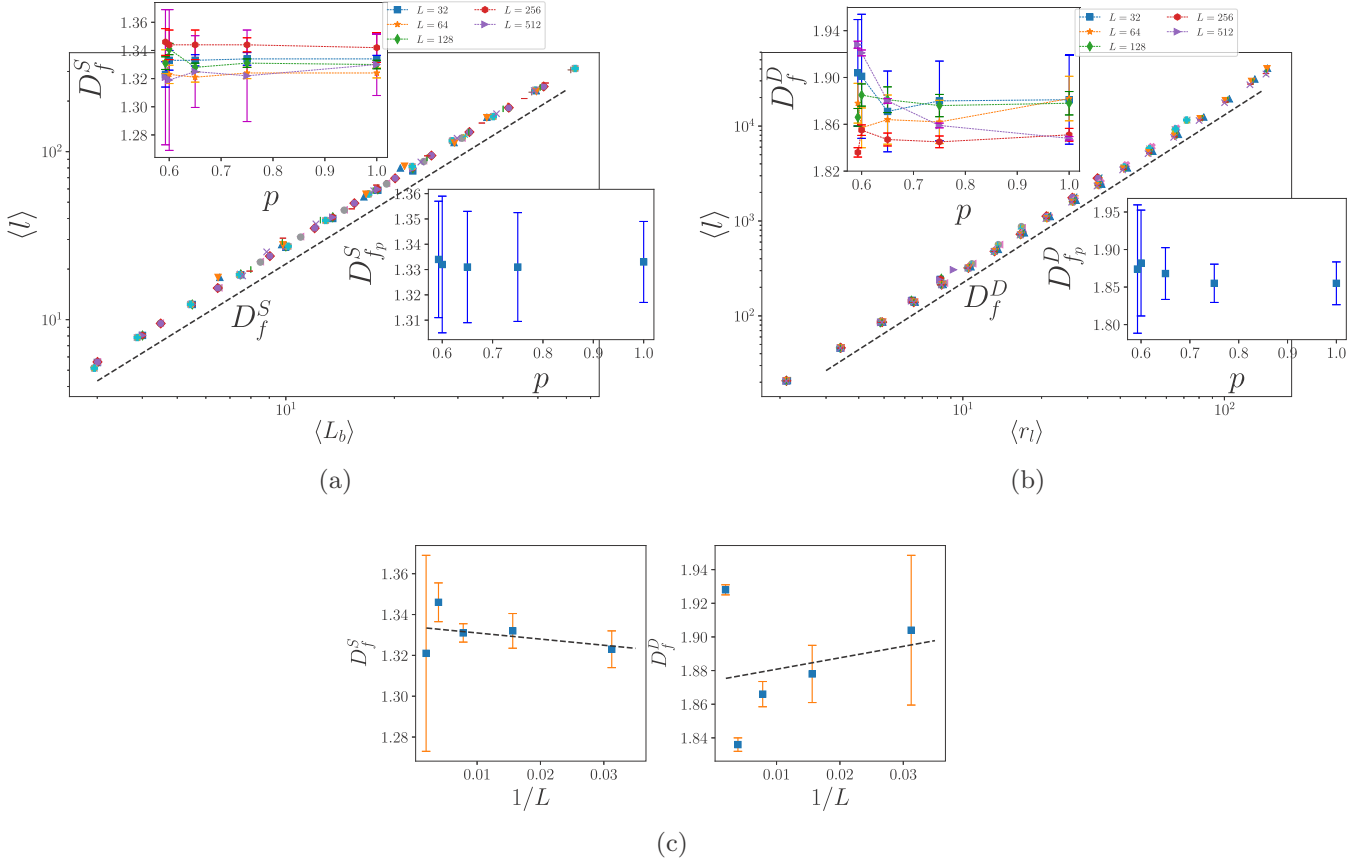


FIG. 2. The numerical results for percolation background: (a) The numerical results of the fractal dimension, which is the slope of the $l - L_b$ graph in the log-log plot; (b) log-log plot of $l - r_l$ graph, where slope is the fractal dimension; and (c) D_f^S and D_f^D in term of $1/L$ for $p = p_c$ ($p_c = 0.59275$).

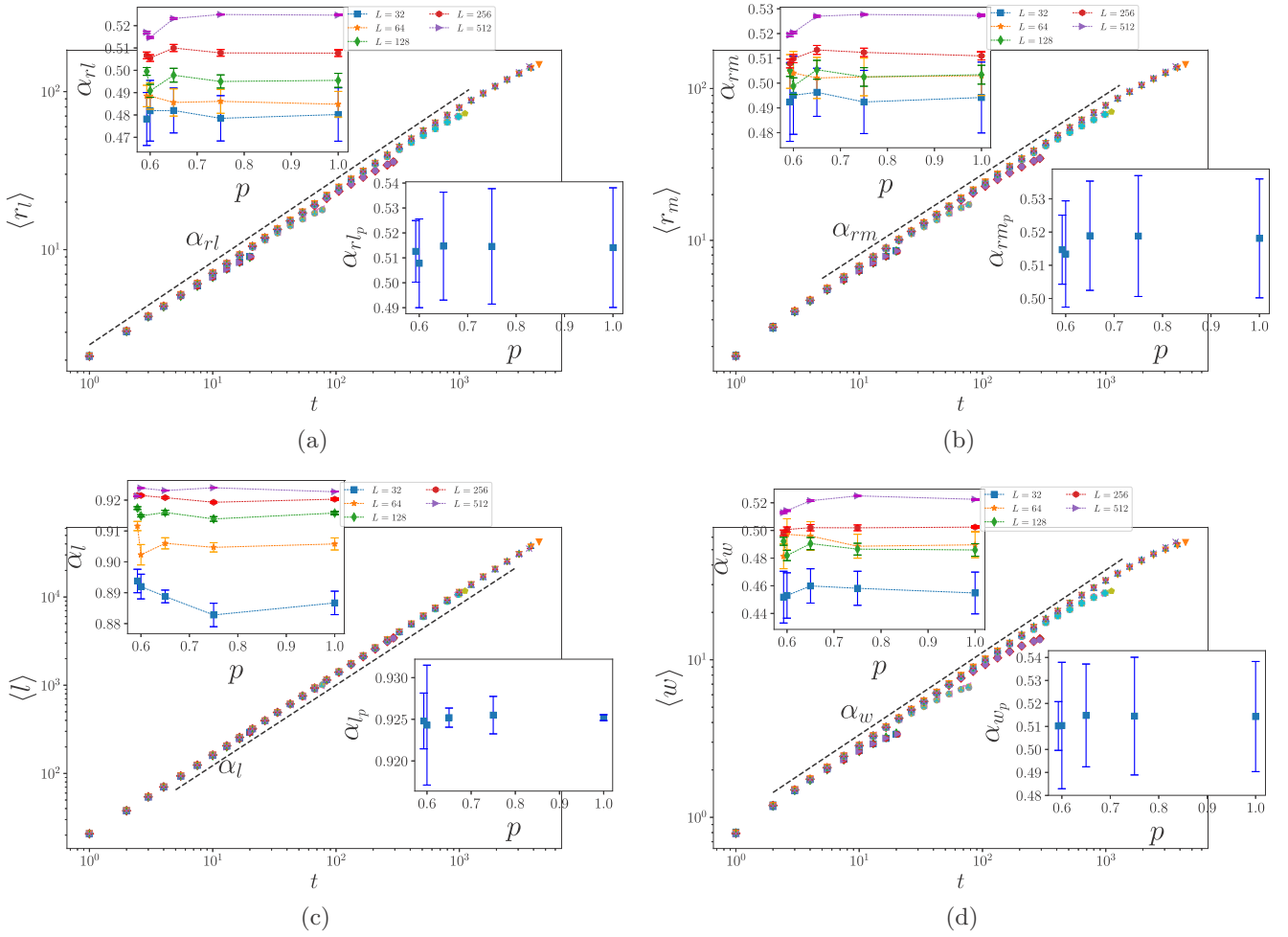


FIG. 3. (a) The time dependence of the average of l . (b) The time dependence of the average of r_l . (c) The time dependence of the average of r_m . (d) The time dependence of the average of w .

In the standard IP model x , $x = w, l, r_l, r_m$ shows power-law behavior with time, reflected in the following relation,

$$\langle x \rangle \propto t^{\alpha_x}, \quad (4)$$

where α_r accounts for the type of diffusion; i.e., for $\alpha_r < \frac{1}{2}$ ($> \frac{1}{2}$) we are in the sub- (super-) diffusion regime, whereas for $\alpha_r = \frac{1}{2}$ we are right in the normal diffusion regime. Two types of fractal dimension can be defined: dynamic fractal dimension (DFD, shown by D_f^D) and static fractal dimension (SFD, shown by D_f^S). The former is defined via the dynamical relation between l and r , i.e., $\langle \log_{10} l(t) \rangle = D_f^D \langle \log_{10} r_l(t) \rangle + cnt$ ($\langle \dots \rangle$ being the ensemble average). For the latter case (SFD), we consider the largest hole of the system in the percolation time (t_{perc}) and extract the fractal dimension of the boundary of the largest hole using the box-counting (BC) scheme to find D_f^S , shown schematically in Fig. 1. The holes of the system are obtained using the Hoshen-Kopelman (HK) algorithm [32]. Importantly, using the HK algorithm, we extracted and analyzed the largest hole for which the fractal dimension is obtained to be D_f^S (ordinary IP) = 1.33 ± 0.01 as expected [14].

In the next subsection, we explain the models used to generate the correlated disorder pattern.

B. Supports: Percolation, Ising, and RCP correlated lattices

Let us give a brief description of the models which are used to simulate the correlated lattices served as the support of IP. The models are listed below.

One-site percolation, which is one of the most important and yet simply defined examples in the critical phenomena, here is employed to fix the impermeable site configuration $\{s_i\}_{i=1}^N$. In this model, we set this configuration at random with an external parameter $0 \leq p \leq 1$: For each site i , we set $s_i = +1$ with probability p and $s_i = -1$ with probability $1 - p$. Many properties of this model are known [33–36], like the facts that it belongs to $c = 0$ conformal field theory [37] and its relations to Coulomb gas [38] and Q -state Potts model [39–41]. In this model, for p values lower than a critical threshold p_c , there is no percolation cluster, whereas for the case $p \geq p_c$ almost definitely we have a percolation cluster. The critical and not-critical properties of this model have been investigated widely in the literature [33,34]. For the square lattice, it is known that $p_c \approx 0.5927$ [42,43]. In

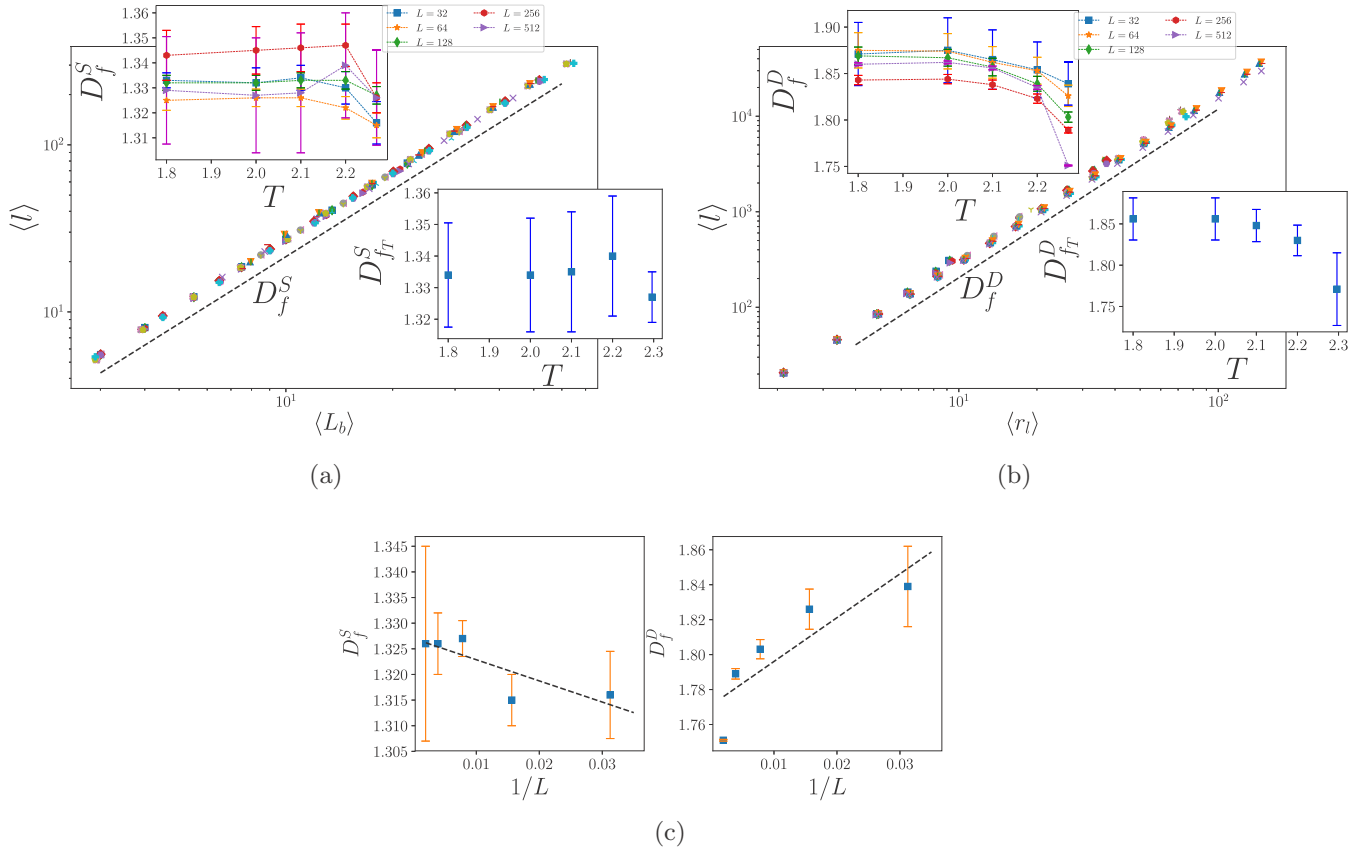


FIG. 4. The numerical results for Ising background: (a) the numerical results of the fractal dimension D_f^S , which is the slope of the $l - L_b$ graph in the log-log plot; (b) log-log plot of $l - r_l$ graph, where slope is the fractal dimension; and (c) D_f^S and D_f^D in term of $1/L$ for $T = T_c$ ($T_c = 2.26918$).

our paper, we consider only the percolated clusters as a host for the IP dynamics. The dynamical aspects of some statistical models have been already studied on the site percolation systems, like sand piles [21,22], self-avoiding walks [28], loop-erased random walks [44], and the Ising model [27]. The case $p \geq p_c$ is considered in this paper, where the fluid moves through the largest percolating cluster.

Two-Ising model has originally been developed for magnetic systems, but we use it to model the impermeable site's configuration. It is a good choice for this study since it (1) is a binary variable, (2) minimally makes the lattice correlated, and (3) has a tuning parameter (artificial temperature T) that controls the correlations. The variables in this model are $s = +1$ and $s = -1$. The interactions in this model are short range (the first neighbor). This model, in the zero magnetic field limit, is described by the following:

$$H = -J \sum_{\langle ij \rangle} s_i s_j, \quad (5)$$

where $\langle ij \rangle$ shows that the summation is over the nearest neighbor sites. The coupling constant J identifies the type of interactions; we consider the ferromagnetic interaction $J_{ij} > 0$. The correlations in this model are tuned by the (here artificial) temperature T . In two dimensions, this model undergoes the magnetic phase transition (from para- to ferromagnetic phase, $T > T_c$ and $T < T_c$ respectively) [27,45,46]. This

phase transition is along with a percolation phase transition in two dimensions; i.e., for $T < T_c$ a percolation geometric cluster is formed which is composed of connected sites with the same spin. We identify such clusters using the HK method [32] and define the IP model on top of this cluster. The dynamical aspects of many statistical models have been already studied on the Ising-correlated lattices, like the sand piles [23,24], self-avoiding walks [28], loop-erased random walks [47], and the Ising model [27]. In all cases, a power-law behavior is seen for the *exponents* in the vicinity of the critical point, which is called “secondary power law” behavior. To generate the Ising samples, we used the Swendsen-Wang algorithm [48] to avoid the critical slowdown problem. In this algorithm, instead of a single spin flip, which is done in the Metropolis method, one flips a connected cluster of Fortuin-Kasteleyn (FK) clusters, which is a geometric connected cluster with the same oriented spins for which the spins are connected with the probability $P_{\text{link}} = 1 - e^{-2/T}$. This approach is proved to be more efficient in the vicinity of the critical points [48].

Three-random Coulomb potential (RCP) is used to make the interactions of the correlated lattice long range. In fact, we consider a quenched correlated system through which the IP dynamics occur. In this model, we generate a Coulomb potential $\phi(\vec{x})$ (\vec{x} represents the points in the system) and use it instead of the uncorrelated random variable r which was introduced in the description of the ordinary IP model. Here

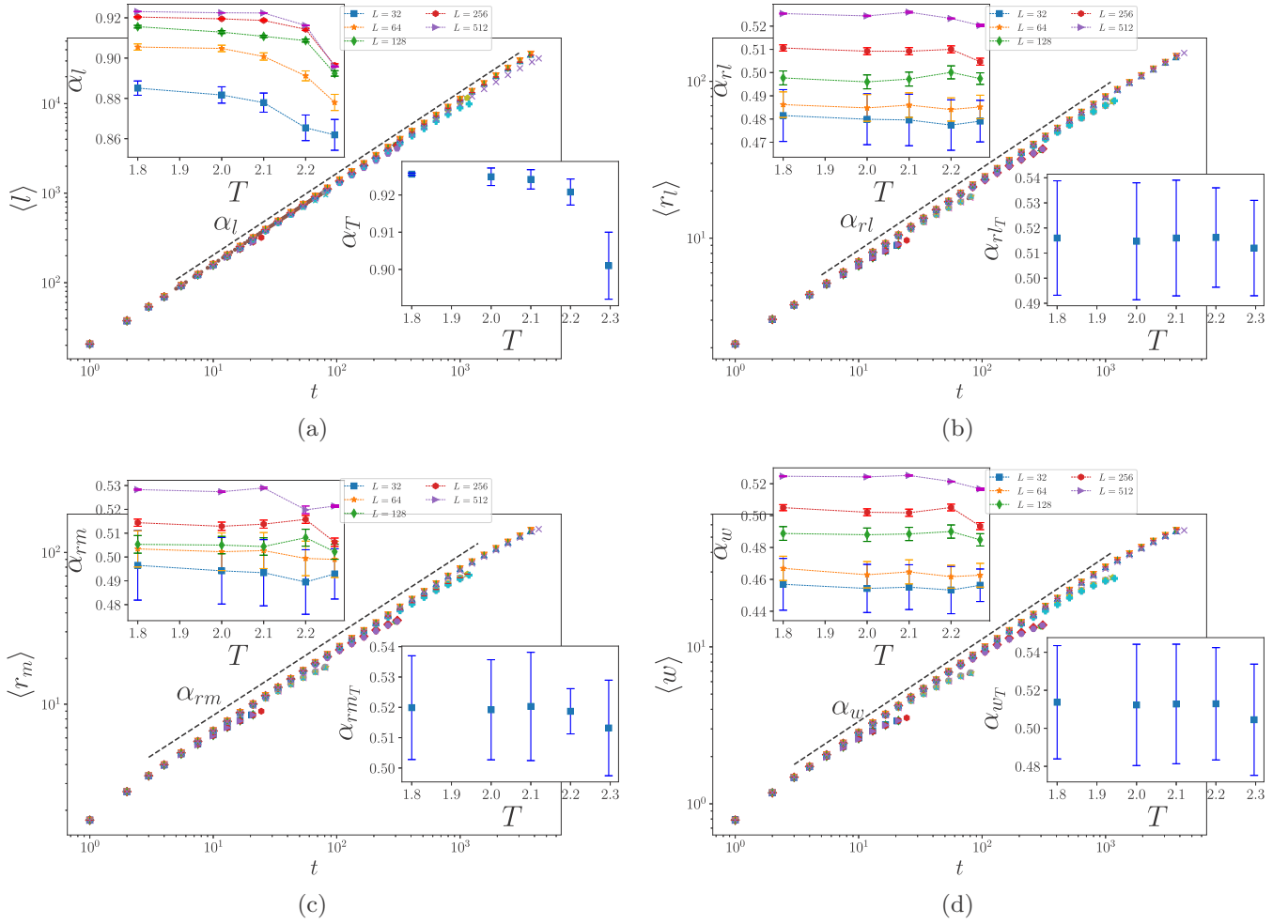


FIG. 5. (a) The time dependence of the average of l . (b) The time dependence of the average of r_l . (c) The time dependence of the average of r_m . (d) The time dependence of the average of w .

we give a brief description of RCP model which is a solution of the Poisson equation. RCP is governed by the following time-independent equation,

$$\nabla^2 \tilde{\phi}(\vec{x}) = -\rho(\vec{x}), \quad (6)$$

which represents the Poisson equation with the dielectric constant $\varepsilon \equiv 1$. In this equation, ρ is a normal distribution time-independent noise with the properties

$$\langle \rho(\vec{x}') \rangle = 0, \quad \langle \rho(\vec{x}) \rho(\vec{x}') \rangle = (n_i a)^2 \delta^2(\vec{x} - \vec{x}'). \quad (7)$$

Also, a is the lattice constant and n_i is the density of Coulomb disorders. We normalize RCP as

$$\phi(\vec{x}) = \frac{1}{2} \left(\frac{\tilde{\phi}(\vec{x})}{\tilde{\phi}_{\max}} + 1 \right), \quad (8)$$

where $\tilde{\phi}_{\max} \equiv \max\{\tilde{\phi}(\vec{x})\}_{\vec{x} \in \text{lattice}}$, so that $\phi(\vec{x})$ becomes correlated variable in the range $[0,1]$. It is worthy to note that a Gaussian distribution cannot be bounded from above or below. This distribution is approximately Gaussian; i.e., for $\phi \ll \phi_{\max}$ it is close to Gaussian distribution. We emphasize that once the solution $\phi(\vec{x})$ is numerically found, we use it as the quenched random variable (instead of r) for the IP dynamics. For generating samples we first, distribute random charges (ρ variable) throughout the square lattice and solve

Eq. (6) using the self-consistent iteration method. The RCP has often been employed as a model to be combined with many other dynamical models, like the percolation [26] and Ising [25] models. For a good review of the RCP model, see Ref. [49].

III. THE NUMERICAL DETAILS AND RESULTS

In this section, we present the results of IP dynamics on the short-range (percolation and Ising) as well as the long-range (RCP) correlated supports. The lattice sizes considered in this work are $L = 32, 64, 128, 256, 512$, and we produced over 10^4 samples for each system size and any control parameter (T for the Ising and p for the percolation). For the Ising model, we considered the temperatures $T = 1.8, 2.0, 2.1, 2.2, 2.26918$, and for the percolation case we have taken into account the occupation probabilities $p = 0.59275, 0.6, 0.65, 0.75, 1.0$. We implemented the model in two separate geometries: $L \times L$ square lattice with free boundary conditions and the cylinder geometry which is used to extract the fractal dimension of the largest hole.

For generating the RCP samples, we used the self-consistent iteration method. In the square lattice, we consider open boundary conditions in both directions, whereas in the

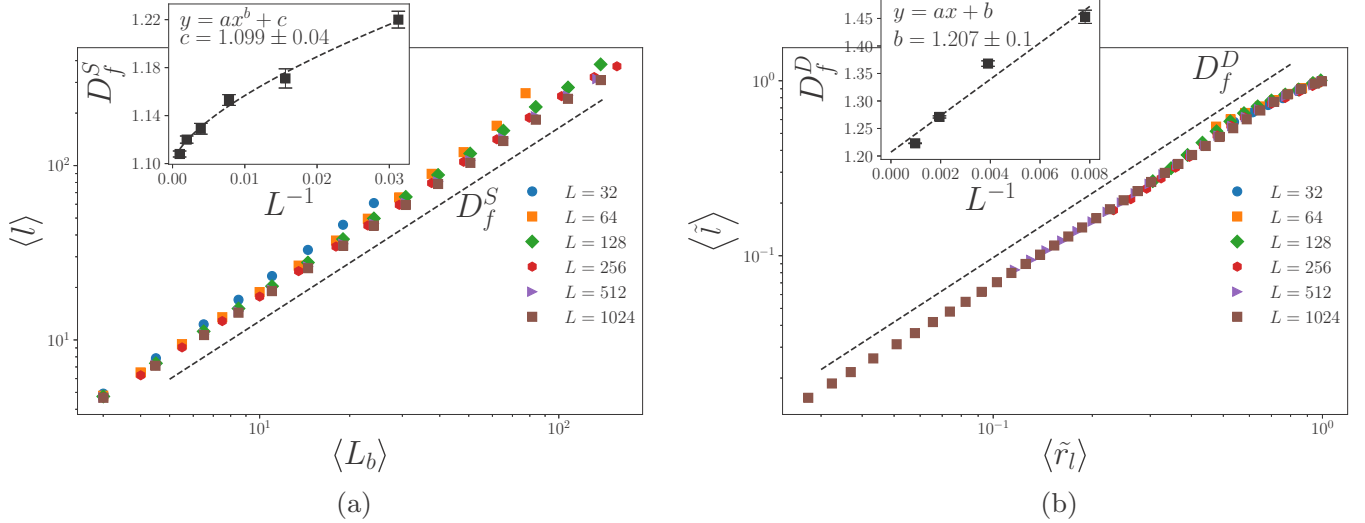


FIG. 6. The numerical results for random Coulomb potential (RCP) background: (a) the numerical results of the fractal dimension, which is the slope of the $l - L_b$ graph in the log-log plot, and (b) log-log plot of $l - r_l$ graph, where slope is the fractal dimension. (Note that in all these insets, x represents the horizontal axis and y represents the vertical axis.)

cylinder geometry we consider the open boundary conditions in one free direction.

1. IP in percolation and Ising-correlated support

The fractal dimension of the boundaries of the largest hole (which is $\frac{4}{3}$ for the regular IP) is the first quantity that we consider here. For the IP percolation, the results are shown in Fig. 2 for $p > p_c$ and all of the L that we use in simulation. The L dependence of the exponent [$D_f^S(L)$] is shown in the upper inset, whereas the lower inset shows the exponent in the thermodynamic limit [$D_f^S(\infty)$], which is obtained using the extrapolation relation

$$D_f^S(L) = D_f^S(\infty) + \frac{A}{L}, \quad (9)$$

where A is a nonuniversal proportionality constant. We see that this exponent (D_f^S) does not significantly run with p being fixed on the theoretical prediction 1.32 ± 0.03 , even in the vicinity of the critical point for which the error bars are higher. In Fig. 2(b), the DFD is reported, for which D_f^D is robust against p and is fixed to 1.9 ± 0.2 . This is due to the fact that a host media with impermeable sites modeled with uncorrelated site percolation is expected to be in the universality class of IP. To understand this, we first notice that an impermeable site does not correspond precisely to an active site with highest r value, i.e., $r = 1$, since the latter can ultimately be occupied with fluid under some *rare* circumstances where there is no other choice for the fluid, e.g., the site with $r = 1$ is completely surrounded by the fluid. Ignoring these rare configurations, which are expected to take place in the very long-time limit (ending time of the process), we can approximately replace an impermeable site with a site with $r = 1$ in the dynamical process. Given this, a host with uncorrelated site percolation corresponds approximately to a media for which we set $r = 1$ for some random sites.

To investigate this more deeply and observe if this robustness is general, we have considered the time dependence of l , r_l , r_m , and w , which are represented in Fig. 3, showing that they behave in a power-law fashion. From Figs. 3(a) and 3(b), we see that the system is in the normal diffusion regime, which is detected by the $r - t$ exponent $\alpha_r = 0.5 \pm 0.05$ for all p values. The exponent α_l should be compatible with the scaling argument

$$l \propto t^{\alpha_l} \propto [t^{\alpha_r}]^{\frac{\alpha_l}{\alpha_r}} \propto r_l^{\frac{\alpha_l}{\alpha_r}}, \quad (10)$$

so that $\alpha_l = D_f^D \alpha_r = 0.9 \pm 0.05$, which is compatible with Fig. 3(c).

In the conventional growth models, the roughness shows power-law behavior in early time stages and enters a stationary regime after a crossover time. In the latter regime, the absolute value of roughness varies with the system size in a power-law form [50,51]. In our model, shown in Fig. 3(d), the roughness exhibits a power-law behavior, and before entering the stationary phase, the process finishes, no matter what the system size is. The exponent of this power-law behavior is $\alpha_w = 0.45 \pm 0.05$, which is almost constant for all p values.

Interestingly we have observed that the correlations due to the short interactions in the Ising model do not change this behavior. The same analysis has been carried out in Figs. 4 and 5. This time, the exponents show robust behavior against $T < T_c$, which controls the range of correlations. The exponents do not significantly change even in the vicinity of the critical temperature. In Figs. 4(a) and 4(b), although the estimated fractal dimensions bind downward in the vicinity T_c , they lie within the error bars of the estimated values at the lower temperatures in the thermodynamic limit [$L \rightarrow \infty$ shown in the lower insets, which has been obtained using the extrapolation relation Eq. (9)]. The extrapolated exponents (thermodynamic limit, shown in the lower insets) that are reported in Figs. 5(a)–5(c), and 5(d) show more robust behavior.

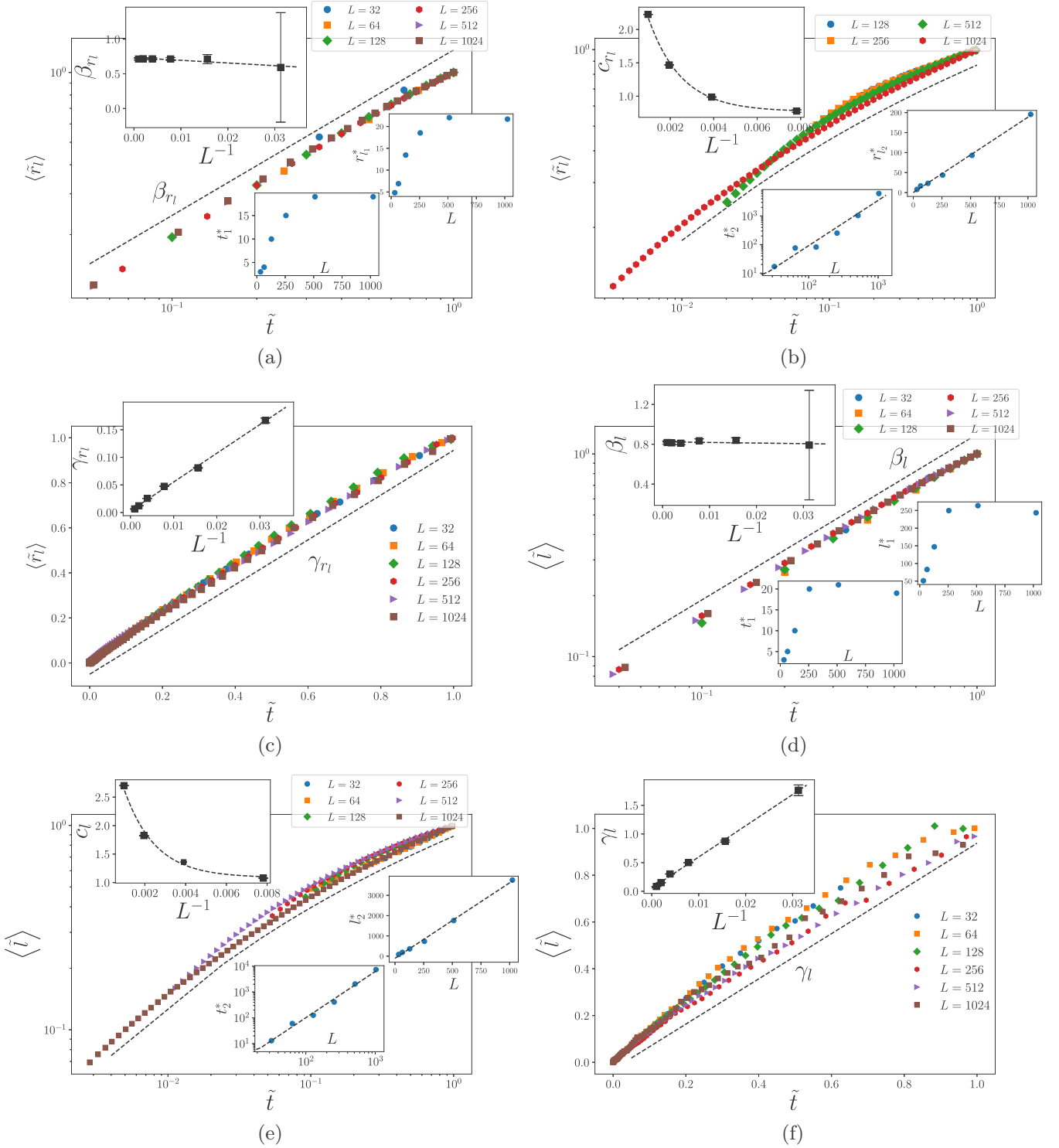


FIG. 7. The numerical results for random Coulomb potential (RCP) background: (a) The time dependence of the average of r_l in the first phase that renormalizes to one. (b) The time dependence of the average of r_l in the crossover area. (c) The time dependence of the average of r_l in the third phase. (d) The time dependence of the average of l in the first phase that renormalizes to one. (e) The time dependence of the average of l in the crossover area. (f) The time dependence of the average of l in the third phase.

Our calculations show that the introduction of uncorrelated (percolation) and correlated (Ising) lattice imperfections with short-range interactions does not change the universality class of the IP model; i.e., it is an irrelevant perturbation for the IP class.

2. IP on random Coulomb potential (RCP) correlated support

The fact that the critical behaviors of IP for $p > p_c$ and $T < T_c$ are similar to the IP model is expected since in these intervals the properties of the host media are identical to the perfect (regular) support in large scales. The only case

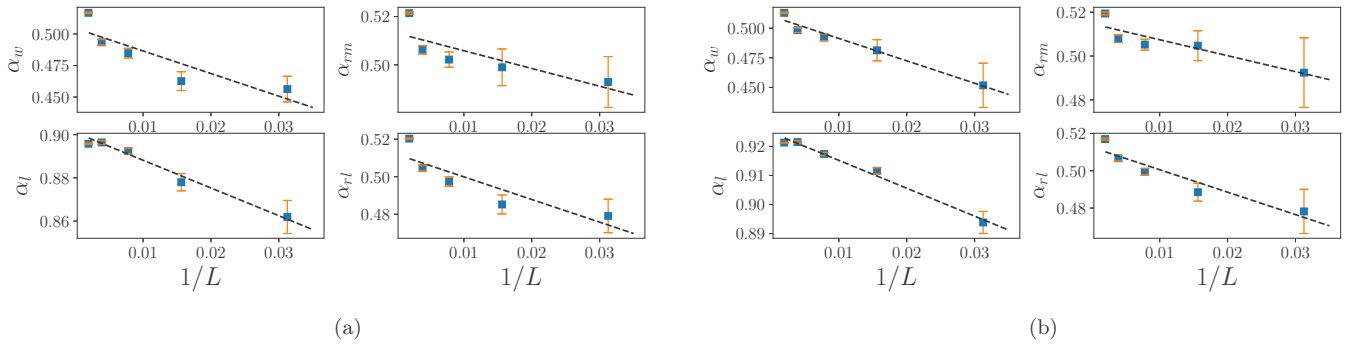


FIG. 8. (a) α_x in term of $1/L$ for $T = T_c$ ($T_c = 2.26918$). (b) α_x in term of $1/L$ for $p = p_c$ ($p_c = 0.59275$). (Note that $x = rl, rm, l, w$.)

where the model has a chance to behave in a different way is right at the critical points, since in this case the host is self-similar and the features of it repeat by rescaling the space. The analysis in the previous section showed, however, that the properties of the model do not change even in the critical points. In RCP (and generally scale-invariant rough surfaces with scale-invariant Lagrangian) the system is always self-similar, and consequently, the correlations are power-law having no referred scale. The difference between the two studied cases (percolation- and Ising-correlated supports) at the critical point is that, here in addition to the long-ranged correlations, the *interactions* are also long-range (Coulomb interactions).

In this section, the *pore quality* is supposed to be described by relation (8), whose correlations are proved to be [25,26]

$$\langle h(\vec{x} + \vec{x}_0)h(\vec{x}) \rangle \propto \log_{10} |x_0|, \quad (11)$$

which is long range. This model is equivalent to a scale-invariant rough surface with zero roughness exponent. The properties of some dynamical models on RCP-correlated supports are already done [25,26].

Here consider IP in support, where r quantity is selected from the solution of Eq. (8). In this case, the critical properties of IP change significantly. Figure 6(a) shows that the SFD in the thermodynamic limit is $D_f^S(L \rightarrow \infty) = 1.099 \pm 0.040$ (see the inset). The dynamic fractal dimension is $D_f^D(L \rightarrow \infty) = 1.207 \pm 0.1$. In this figure, we have used normalization to one, where the numbers on each axis are divided by their maximum (end point). Note that each graph including \tilde{x} or

\tilde{y} symbol is normalized to one. Both of these exponents are significantly different from the ordinary IP model. This leads us to an important conclusion: Long-range correlations for SRI models is necessary for bringing it out from the ordinary IP universality class (see the results in the vicinity of the critical points for the percolation and Ising-correlated supports), while for the LRI case, the properties of the system are very different from those of the ordinary IP universality class.

To be more precise, let us consider the dynamic aspects of the model. We have observed three distinct temporal regimes in the system. For sufficiently small times (power-law regime where $t < t_1^*$), the observables show power-law behavior with time, whereas for intermediate times (logarithmic regime where $t_1^* < t < t_2^*$) it varies with the logarithm of time, and for long times (linear regime where $t > t_2^*$) it changes linearly with time with a slope tending to zero in the thermodynamic limit.

Figure 7(a) shows the gyration radius versus time in the power-law regime, in which it is interestingly seen that $\alpha_{r_l}^{\text{RCP}}(L \rightarrow \infty) = 0.73 \pm 0.04$; i.e., the system is superdiffusive. This should be compared with ordinary IP, which is diffusive (see the previous section). We call the second regime the logarithmic regime since the observables behave like the following relation in this regime

$$\langle x \rangle = a(\log_{10}(t + b))^{c_x}, \quad (12)$$

where a and b are some unimportant constants, and c_x is an exponent. Figure 7(b) shows the results for r_l in this regime, from which we observe that c_{r_l} becomes 0.77 ± 0.2 in the

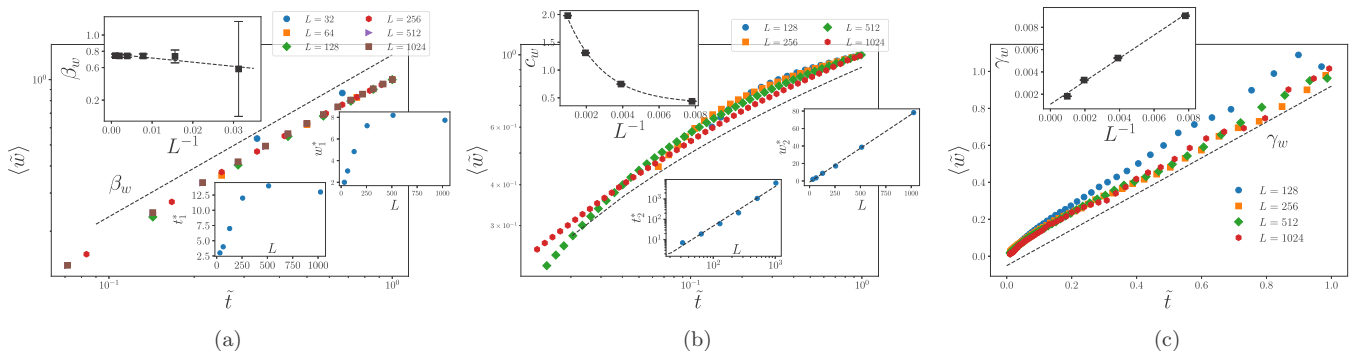


FIG. 9. The numerical results for random Coulomb potential (RCP) background: (a) The time dependence of the average of w in the first phase that renormalizes to one. (b) The time dependence of the average of w in the crossover area. (c) The time dependence of the average of w in the third phase.

thermodynamic limit. The lower inset shows that t_2^* goes to infinity faster than t_1^* as $L \rightarrow \infty$, showing that this regime dominates in the thermodynamic limit. The linear regime is described by the linear relation

$$\langle x \rangle = \gamma_x t + b, \quad (13)$$

where γ_x is the slope, shown in the upper inset of Fig. 7(c) which extrapolates to zero in the $L \rightarrow \infty$ limit for r_l . In this figure, we have plotted renormalized $\tilde{Y} = \frac{Y}{Y_{\max}}$ versus $\tilde{X} = \frac{X}{X_{\max}}$, where $Y \equiv \frac{y-y^*}{\gamma_l}$, $X \equiv x - x^*$, and (x^*, y^*) is crossover point. This analysis shows that the linear regime is actually a stationary regime in the thermodynamic limit. The reason is that, as the slope of the graphs tends to zero [see, for example, the inset of Fig. 9(c)] in the thermodynamic limit (in a power-law fashion) the observables become asymptotically nearly constant for the third regime, signaling a stationary regime.

The same features are seen for l in Figs. 7(d), 7(e) and 7(f), from which we see that $\alpha_l^{\text{RCP}} \rightarrow 0.82 \pm 0.03$, $c_l \rightarrow 1.09 \pm 0.35$, and $\gamma_l \rightarrow 0$ in the limit $L \rightarrow \infty$. The same analysis for w shows the same behaviors, with the exponents $\alpha_w^{\text{RCP}} \rightarrow 0.76 \pm 0.05$, $c_w \rightarrow 0.4 \pm 0.2$, and $\gamma_w \rightarrow 0$ in this limit.

IV. CONCLUSION

In the present paper, to get closer to the real fluid dynamics in a porous medium, we considered the effect of the pattern of the impermeable pores of the background on top of which the invasion percolation (IP) is defined. For the model for the sedimentation process, we defined three different models to obtain the pattern of impermeable sites. Ordinary and Ising-correlated percolation models were exploited which include short-range interactions (SRI; note that for the uncorrelated percolation the interaction range is zero, while for the Ising-correlated the interaction is limited to the first neighbor), and a random Coulomb potential was employed as a representative of models with long-range interactions (LRI). Various statistical observables were studied, among which are the gyration, the loop length, and the mass of the external perimeter of the growing cluster. The critical exponents for SRI are nearly identical to the values for ordinary IP far from the critical points. For the uncorrelated percolation, up to our estimations,

the exponents do not show a serious change even in the vicinity of the critical point p_c , while for the Ising-correlated case, the exponents show deviations in the vicinity of the critical point $T = T_c$. The situation is completely different for the LRI case, for which the exponents are very different with respect to the ordinary IP case. For example, the fractal dimension of the external perimeter of the largest hole (which is $\frac{4}{3}$ for the ordinary IP) reduces to $D_f = 1.099 \pm 0.04$. This shows that the response of the dynamical model to the structure of the background depends on the range of interactions and also the correlation length of the spatial configuration of impermeable regions so that larger range of interactions corresponds to stronger effect of background pattern and higher deviations of the exponents with respect to the ordinary IP. The correlation length of the background permeability field is largest in the vicinity of the critical points, where the deviation of the exponents are high for the Ising-correlated case.

We tested also the dynamical properties of the model. For the uncorrelated percolation case, the growth exponents are robust against p , but for the Ising model, the exponents are significantly different only in the vicinity of the critical point. For the RCP, the situation is different and the exponents are completely different. Three regimes were found for the latter case: the power law (small time), the logarithmic (moderate time), and the linear (long time) regimes. While the first crossover time is shown to be finite in the thermodynamic limit, the second crossover time goes to infinity, which reveals that the *logarithmic regime is dominant in the thermodynamic limit*. Some of the observables become nearly constant in the thermodynamic limit for the long-time regime, although this regime disappears in the thermodynamic limit.

APPENDIX: SOME OF THE GRAPHS

For more details on short-range notion background, you can refer to Fig. 8 to see the fit α_x in terms of $1/L$ for T_c and p_c . Also, because of the similar behavior of all dynamic processes in the random Coulomb potential background, we present graphs of the roughness and radius of mass gyrus for all three elementary, middle, and final times in this Appendix (Figs. 9 and 10).

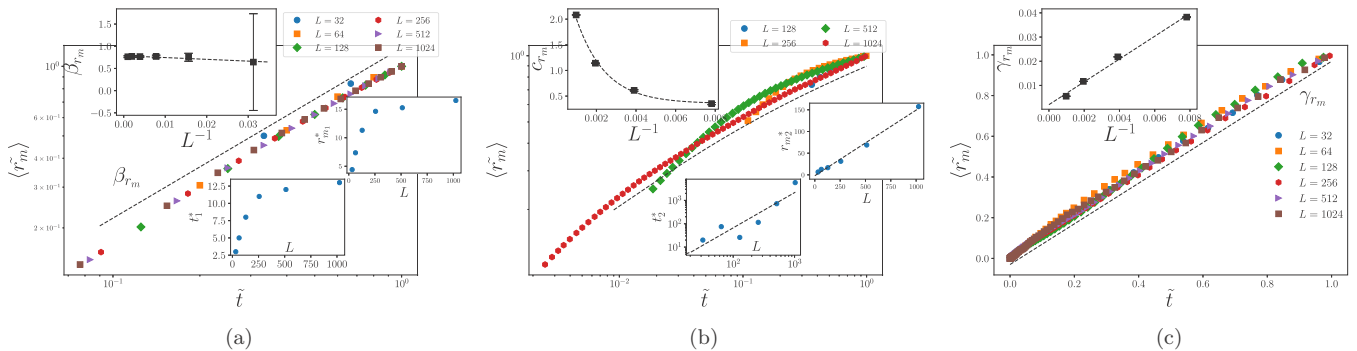


FIG. 10. The numerical results for random Coulomb potential (RCP) background: (a) the time dependence of the average of r_m in the first phase that renormalizes to one; (b) the time dependence of the average of r_m in the cross-over area; and (c) the time dependence of the average of r_m in the third phase.

- [1] R. Chandler, J. Koplik, K. Lerman, and J. F. Willemsen, *J. Fluid Mech.* **119**, 249 (1982).
- [2] D. Wilkinson and J. F. Willemsen, *J. Phys. A: Math. Gen.* **16**, 3365 (1983).
- [3] C. P. Stark, *Nature (London)* **352**, 423 (1991).
- [4] P.-G. de Gennes and E. Guyon, *J. Mec.* **17**, 403 (1978).
- [5] R. Lenormand and S. Bories, *CR Acad. Sci.* **291**, 279 (1980).
- [6] R. Lenormand and C. Zeccone, *Phys. Rev. Lett.* **54**, 2226 (1985).
- [7] R. Engelman and Z. Jaeger, *Fragmentation, Form, and Flow in Fractured Media* (Adam Hilger, London, England, 1986).
- [8] C. S. Parkhurst, W. F. Doyle, L. A. Silverman, S. Singh, M. P. Anderson, D. McClurg, G. E. Wnek, D. R. Uhlmann, C. J. Brinker, D. E. Clark *et al.*, in *Materials Research Society Symposium Proceedings* (MRS, Pittsburgh, Pennsylvania, 1986), Vol. 73, p. 769.
- [9] L. Xu, S. Davies, A. B. Schofield, and D. A. Weitz, *Phys. Rev. Lett.* **101**, 094502 (2008).
- [10] A. Vidales, E. Miranda, M. Nazzarro, V. Mayagoitia, F. Rojas, and G. Zgrablich, *EPL* **36**, 259 (1996).
- [11] T. Babadagli, *Phys. A (Amsterdam, Neth.)* **285**, 248 (2000).
- [12] M. A. Knackstedt, M. Sahimi, and A. P. Sheppard, *Phys. Rev. E* **65**, 035101(R) (2002).
- [13] K. Peter and M. Mohsen, *Percolation Theory in Reservoir Engineering* (World Scientific, Singapore, 2018).
- [14] S. Tizdast, Z. Ebadi, N. Ahadpour, M. Najafi, and H. Mohammadzadeh, *Phys. Scr.* **95**, 115212 (2020).
- [15] J. Feder, *New York* **9**, 279 (1988).
- [16] S. Roux and E. Guyon, *J. Phys. A: Math. Gen.* **22**, 3693 (1989).
- [17] L. Furuberg, J. Feder, A. Aharony, and T. Jøssang, *Phys. Rev. Lett.* **61**, 2117 (1988).
- [18] M. Najafi and M. Ghaedi, *Phys. A (Amsterdam, Neth.)* **427**, 82 (2015).
- [19] C. Oliveira, A. Araújo, L. Lucena, M. Almeida, and J. Andrade Jr., *Phys. A (Amsterdam, Neth.)* **391**, 3219 (2012).
- [20] W. Li, J. L. Jensen, W. B. Ayers, S. M. Hubbard, and M. R. Heidari, *J. Petroleum Sci. Eng.* **68**, 180 (2009).
- [21] M. Najafi, *J. Phys. A: Math. Theor.* **49**, 335003 (2016).
- [22] M. Najafi and H. Dashti-Naserabadi, *J. Stat. Mech.: Theory Exp.* (2018) 023211.
- [23] J. Cheraghalizadeh, M. N. Najafi, H. Dashti-Naserabadi, and H. Mohammadzadeh, *Phys. Rev. E* **96**, 052127 (2017).
- [24] M. N. Najafi, J. Cheraghalizadeh, M. Luković, and H. J. Herrmann, *Phys. Rev. E* **101**, 032116 (2020).
- [25] J. Cheraghalizadeh, M. N. Najafi, and H. Mohammadzadeh, *Eur. Phys. J. B* **91**, 81 (2018).
- [26] J. Cheraghalizadeh, M. Najafi, and H. Mohammadzadeh, *J. Stat. Mech.: Theory Exp.* (2018) 083301.
- [27] J. Cheraghalizadeh and M. N. Najafi, *Phys. Rev. E* **98**, 052136 (2018).
- [28] J. Cheraghalizadeh, M. N. Najafi, H. Mohammadzadeh, and A. Saber, *Phys. Rev. E* **97**, 042128 (2018).
- [29] P. Claudin, F. Charru, and B. Andreotti, *J. Fluid Mech.* **671**, 491 (2011).
- [30] S. Mukhopadhyay and M. Sahimi, *Chem. Eng. Sci.* **55**, 4495 (2000).
- [31] M. A. Knackstedt, S. Marrink, A. P. Sheppard, W. V. Pinczewski, and M. Sahimi, *Transp. Porous Media* **44**, 465 (2001).
- [32] J. Hoshen and R. Kopelman, *Phys. Rev. B* **14**, 3438 (1976).
- [33] W. Werner, *Statistical Mechanics* (American Mathematical Society, Institute for Advanced Study, USA, 2009).
- [34] S. Smirnov and W. Werner, *Math. Res. Lett.* **8**, 729 (2001).
- [35] R. Langlands, P. Pouliot, and Y. Saint-Aubin, *Bull. AMS* **30**, 1 (1994).
- [36] J. Cardy, *arXiv:math-ph/0103018*.
- [37] P. Mathieu and D. Ridout, *Phys. Lett. B* **657**, 120 (2007).
- [38] W. R. Clarke, C. E. Yasin, A. R. Hamilton, A. P. Micolich, M. Y. Simmons, K. Muraki, Y. Hirayama, M. Pepper, and D. A. Ritchie, *Nat. Phys.* **4**, 55 (2008).
- [39] R. B. Potts, in *Mathematical Proceedings of the Cambridge Philosophical Society* (Cambridge University Press, Cambridge, UK, 1952), Vol. 48, pp. 106–109.
- [40] F.-Y. Wu, *Rev. Mod. Phys.* **54**, 235 (1982).
- [41] J. Essam, *J. Math. Phys.* **20**, 1769 (1979).
- [42] K. Malarz and S. Galam, *Phys. Rev. E* **71**, 016125 (2005).
- [43] M. Majewski and K. Malarz, *Acta Phys. Pol. B* **38**, 2191 (2007).
- [44] E. Daryaei, *Phys. Rev. E* **90**, 022129 (2014).
- [45] R. Baierlein, *Thermal Physics* (American Association of Physics Teachers, 1999).
- [46] G. Gallavotti, in *Statistical Mechanics* (Springer, Berlin, 1999), pp. 175–207.
- [47] J. Cheraghalizadeh and M. N. Najafi, *Phys. Scr.* **94**, 095204 (2019).
- [48] R. H. Swendsen and J.-S. Wang, *Phys. Rev. Lett.* **58**, 86 (1987).
- [49] S. Sheffield, *Probab. Theory Relat. Fields* **139**, 521 (2007).
- [50] J. Kondev, C. L. Henley, and D. G. Salinas, *Phys. Rev. E* **61**, 104 (2000).
- [51] A.-L. Barabási and H. E. Stanley, *Fractal Concepts in Surface Growth* (Cambridge University Press, Cambridge, 1995).